A Photonic Link at 4.7 K with >1 GHz bandwidth towards an Optical Quantum Computing Interface

Santosh Mutum[1], Patrick Vliex[1], Jonas Bühler[1], Dennis Nielinger[1], Mario Schlösser[1], Stefan van Waasen[12]
[1]Peter Grünberg Institute - Integrated Computing Architectures - ICA | PGI-4,
Forschungszentrum Jülich, Germany
[2]Faculty of Engineering, Communication Systems, University of Duisburg-Essen, Germany
{s.mutum, p.vliex, j.buehler, d.nielinger, m.schloesser, s.van.waasen}@fz-juelich.de

***Abstract* — This paper presents the results of a performance evaluation of a photonic link in a cryogenic environment. The transmission from room temperature to 4.7 K was achieved using a 904 nm and 1310 nm lasers with a bandwidth exceeding 1 GHz using both silicon-based and InGaAs-based commercial photodiodes. A reduction in DC photocurrent was observed. Moreover, the frequency response measurements demonstrate that both photodiodes improve their maximum bandwidth even when unbiased at cryogenic environment. Furthermore, this work presents a demonstration of photonic control of cryogenic electronics for quantum computing applications.**

***Keywords* — photonic system, cryogenics, laser, photodiodes, quantum, data link.**

I. Introduction

The latest generation of quantum processors boasts an increased number of qubits, enhanced coherence times, and optimized error correction capabilities. The issue of scalability remains a significant challenge for all platforms, particularly in regard to interconnects and control systems [1]. As the number of qubits increases, the cables that are crucial for transmitting microwave signals become unwieldy. This poses limitations due to physical space, heat dissipation, and interference management. The complexity and the associated microwave control hardware also increase with the addition of each new qubit, creating foreseeable bottlenecks in signal integrity and synchronization. To address these issues, research is being conducted into innovative solutions such as cryogenic multiplexing and advanced materials for cabling. Furthermore, cryogenic CMOS technology is of great significance for quantum hardware, as it allows for the low-temperature control of qubits [2]. Advances in cryogenic amplifiers, memory elements, and control systems have the effect of minimizing thermal noise and power consumption, thereby enhancing qubit fidelity and reducing wiring complexity [3]. Another promising development is the use of deep cryogenic photonic links, which employ lasers and optical fibers for qubit control [4]. Meanwhile, radio frequency (RF) photonics, which was previously a niche technology, has become a vital component in communications [5]. This is due to the fact that RF photonic systems have high bandwidth and low interference, which are essential for next-generation wireless communication [6] and even quantum computing. In this paper, Section II describes the implementation of a cryogenic photonic link and the theory of photodiode behaviour in a cryogenic environment, while Section III shows the experimental setup. Section IV presents the corrrsponding measurement results and Section V provides a conclusion.

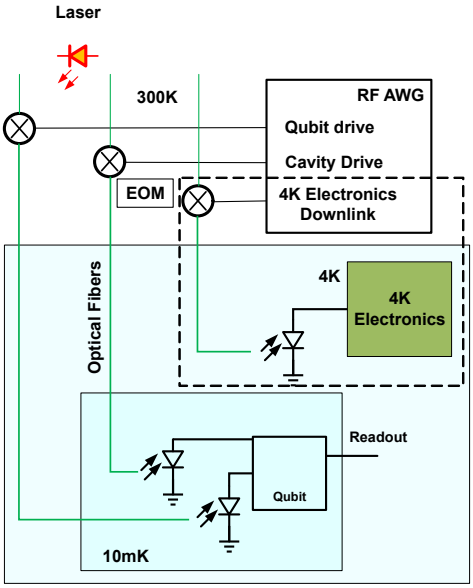

Fig. 1. Concept of photonic link with a qubit and electronics at 4K as presented in [7]

II. Cryogenic Photonic Link

By leveraging on the well-established field of RF photonics and its dependable room temperature performance, a cryogenic photonic system presents a promising solution to the challenges inherent to quantum computing and other high-performance applications that necessitate ultra-low temperatures for qubit functionality [4]. This approach benefits from the high bandwidth, low latency, and immunity to electromagnetic interference which are crucial for guaranteeing qubit coherence and fidelity [7]. In the proposed design, the transmission process entails modulating a laser at room temperature and transmitting the optical signal to the cryogenic temperature level. Commercial photodiodes are employed to

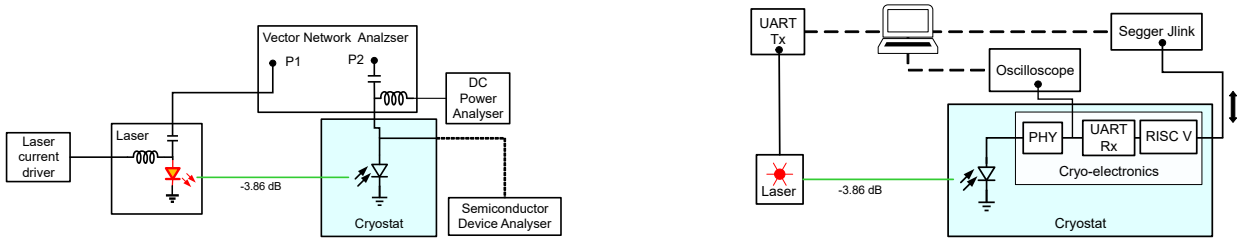

Fig. 2. Detailed measurement setup. a) For DC measurement and frequency response measurement by direct modulation. b) For controlling cryo electronics via photonic link.

convert the signal to a baseband signal, which is then utilized for electronic and qubit interactions as shown in Fig. 1. The key performance factors for the cryogenic photodiode include efficiency, power consumption, and heat dissipation. In this work we focus on the down-link path into the 4 K stage. The behavior and performance of different photodiodes in terms of DC characteristics and high-frequency response at low temperatures under various biasing conditions are investigated.

A. *Theory of photodiodes characteristics in cryogenics*

Performance factors for photodiodes include efficiency, responsivity, dark current, response time, and bandwidth. The IV curve allows for the extraction of open-circuit voltage (V_{oc}) and short-circuit current (I_{sc}), with I_{sc} directly linked to both responsivity and quantum efficiency η. V_{oc}, on the other hand, is indirectly influenced by these parameters through I_{sc}. Theoretically, I_{sc} stays relatively constant with temperature for a typical photodiode at a given optical power and wavelength due to minimal temperature effects on quantum efficiency η. However, the reduced phonon population at lower temperatures decreases quantum efficiency in indirect bandgap photodiodes. Additionally, as temperature drops, the saturation current (I_o) declines, which leads to an increase in V_{oc} due to its logarithmic dependence on I_{sc}/I_o [8]. At cryogenic temperatures, V_{oc} rises while I_{sc} decreases, with the reduction more pronounced in indirect bandgap materials like silicon.

The photodiode bandwidth is influenced by transit time and the RC time constant. The transit-time limited bandwidth depends on the carrier's saturation velocity, while the RC limited bandwidth is inversely related to the RC constant, $f_{RC} = 1/2\pi RC$ where R represents load resistance and C is dominated by the junction capacitance C_j [9]. The overall bandwidth is determined by the lesser of the two limits, but at cryogenic temperatures, improved carrier mobility tends to make the RC limit more critical. C_j varies with the depletion width and area of the photodiode, decreasing as reverse bias (V_{bias}) increases due to the widening depletion width, $d \propto \sqrt{V_i - V_{\text{bias}}}$. At cryogenic temperatures, the depletion width expands further due to a higher built-in potential, $V_i \propto \ln\left(\frac{1}{n_i^2}\right)$, caused by a lower intrinsic carrier concentration (n_i) [10], enhancing the electric field across the junction. Thus, at cryogenic conditions and given a certain bias, even at zero bias, photodiode bandwidth significantly improves.

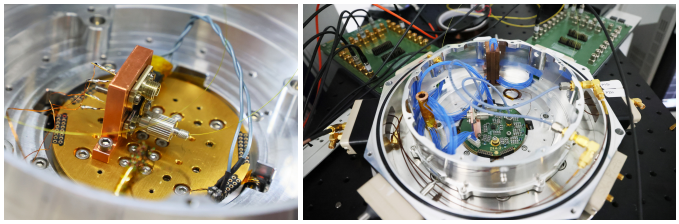

Fig. 3. Experimental setup showing photodiode characterization and photonic control electronic system in the cryostat.

III. Setup

The experimental setup utilized an Attocube attodry800 closed cycle helium cryostat, achieving a base temperature of 4.7 K for sample cooling. An 904 nm and 1310 nm laser was employed, operating within the milliwatt range, and a bias tee enabled direct modulation up to 1 GHz, limited by the used Thorlabs LDM9LP modulator. Two commercial photodiodes from Thorlabs, silicon-based FDS02 and InGaAs based FGA01 were tested inside the cryostat at variable temperatures. For DC measurements, the photodiode's output was connected to high resolution source measure unit (SMU) of Keysight B1500A Semiconductor Device Analyzer, facilitating IV curve generation. For AC measurements, the photodiode's output was linked to port 2 of Agilent Technologies PNA-X N5242A Vector Network Analyser (VNA), which included an integrated bias tee for external biasing, while port 1 of the VNA controlled the laser's direct modulation biasing, as shown in Fig. 2a. The S21 measurement path for direct modulation comprised the laser, fibers, connectors, cryostat feedthrough, and photodiode. Measurements were conducted from 10 MHz to 1 GHz in 5 MHz increments, with fourfold averaging and smoothing applied, with insertion power losses of −3.85 dB in fibers, connectors, and feedthrough. The temperature was varied from 300 K to 4.7 K, and a negative bias voltage range of 0 V to 4 V was applied to the photodiode inside the cryostat. Junction capacitance values for the photodiode were derived from S22 at −20 dBm, averaged around 500 MHz for different bias voltages. To demonstrate the operation of a photonic-controlled cryogenic electronic circuit, the UART Tx output is connected to a laser, as depicted in Fig. 2b. An unbiased photodiode interfaces with the cryogenic IC, which includes an analog frontend consisting of TIA and amplifier along with a RISC-V processor [11]. The analog output is

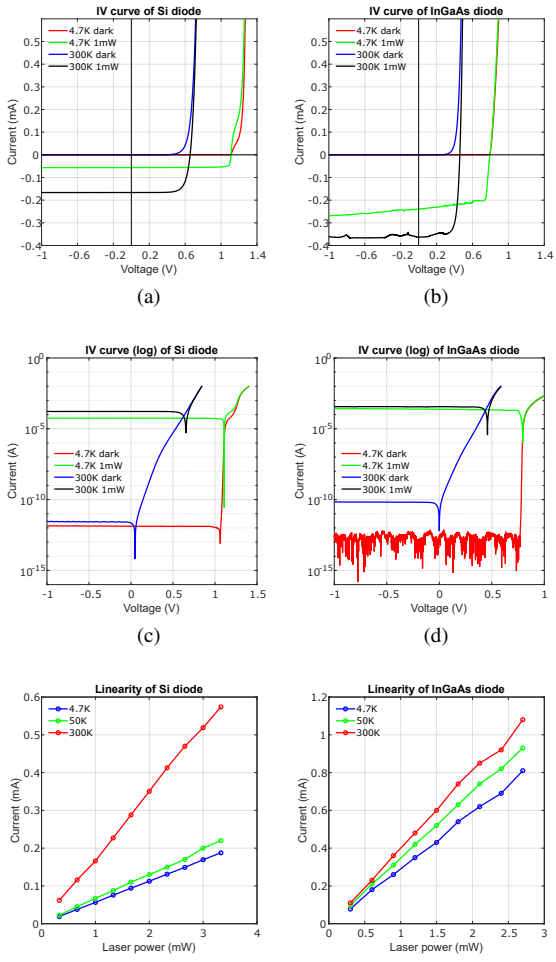

Fig. 4. DC measurement results a) and b) are IV curves of Si and InGaAs photodiodes under investigation both in the dark and with 1 mW laser power. c) and d) are IV curves in logarithmic current as well as e) and f) are linearity of the response as laser power varies respectively.

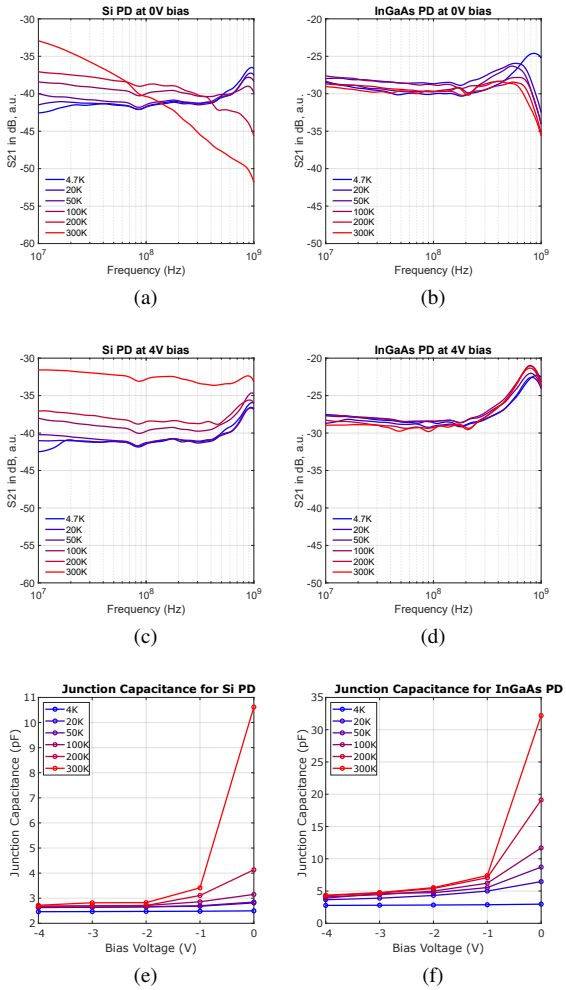

Fig. 5. Frequency response measurement results a) and b) are S21 of Si and InGaAs photodiodes under investigation respectively under 0V reverse bias voltage. c) and d) are S21 of Si and InGaAs under 4 V reverse bias voltage. The measurements are done at 1 mW of optical power with −5 dBm RF power from VNA. e) and f) Junction capacitance extracted from S22 for Si and InGaAs photodiode under investigation.

subsequently connected to an oscilloscope for monitoring purposes. A predefined task is programmed into the processor through a photonic link, and the on-chip JTAG interface is employed to read out the corresponding data.

IV. Result

From Fig. 4a and 4c, a marked increase in V_{oc} is observed, rising from 0.7 V at room temperature to 1.2 V, while I_{sc} decreases from ≈165 µA to ≈60 µA at 4.7 K and 1 mW optical power. Additionally, dark current is reduced. Fig. 4e shows a noticeable drop in DC current at 4.7 K due to reduced phonon availability in the indirect bandgap nature of silicon. Similarly, as in Fig. 4b and 4d for the InGaAs photodiode, the open-circuit voltage increases from 0.4 V at room temperature to 0.8 V at 4.7 K, with reductions in both dark currents and I_{sc} from ≈400 µA to ≈300 µA under 1 mW optical power. Fig. 4f shows less DC current reduction at cryogenic temperatures compared to the Si photodiode due to its direct bandgap.

The S21 measurements from direct laser modulation, as shown in Fig. 5a, demonstrate an increase in bandwidth for the silicon photodiode at cryogenic temperatures, particularly at 0 V bias, alongside a reduction in received power. Applying a 4 V reverse bias, as shown in Fig. 5b, further enhances both the bandwidth and power. Similarly, the S21 measurements for the InGaAs photodiode, shown in 5c and 5d, reveal a comparable trend, though with reduced measured power. The reduction in received RF power which are more pronounced in the Si photodiode improves with applied bias voltage. As illustrated in 5e and 5f, the junction capacitance of both diodes decreases with lower temperatures and higher bias voltages. At 0 V, the silicon photodiode's capacitance drops from ≈10.5 pF at room temperature to ≈2.5 pF at 4.7 K. Similarly, the InGaAs photodiode shows a reduction from ≈32 pF to ≈4.8 pF. Table 1 shows the recent application of photonic links in cryogenics: as a current source, a qubit driver, photonic ICs and this work.

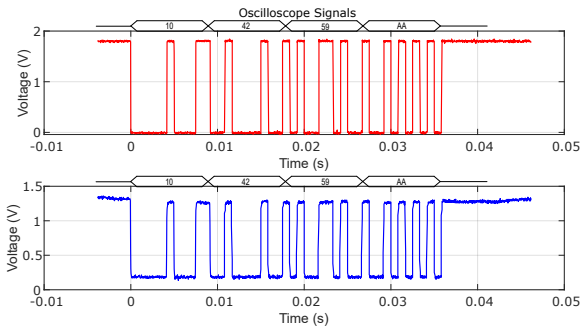

Fig. 6. Digital data sent via UART Tx (red) from room temperature to photonics and received in UART Rx (blue) inside cryostat, see Fig. 2b. An initial demonstration; a lower data rate was utilized, as the RISC-V processor was not specifically designed to support high data rates. The experiment shows a working optical link into the RISC-V processor.

Table 1. Comparison of photodiode parameters at cryogenic temperatures.

Parameters	**[12] 2018**	**[4] 2020**	**[13] 2024**	**This work**
Temperature	4 K	20 mK	11 K	4.7 K
PD type	InGaAs	InGaAs	Ge on Si	Si & InGaAs
Wavelength (nm)	1310	1490	1550	904 & 1310
Bandwidth	14 GHz	5 GHz	-	> 1 GHz

Fig. 6 presents the oscilloscope data successfully transmitted to the processor via the photonic link. The signal remains sufficient to write data to the processor. The written data is subsequently retrieved using the JTAG interface.

V. Conclusion

In this work, a cryogenic photonic link that demonstrates the behavior of commercial Si and InGaAs photodiodes at 4.7 K, also an interface of unbiased photodiode with the cryogenic IC is demonstrated. The IV characteristics, linearity, and frequency response of these photodiodes were assessed using a network analyzer and semiconductor device analyzer. Findings show that bandwidth increases at cryogenic temperatures with reduced current, especially at 0 V bias, mainly due to the temperature-dependent reduction in junction capacitance. Overall, in cryogenic environments, both photodiodes exhibit increased bandwidth, with InGaAs showing lower power reduction compared to Si, while Si technology remains more cost-effective and is readily integrated into photonic chips. Recent measurements utilizing an optical attenuator demonstrate that photodiodes maintain optimal performance at reduced optical power levels down to 1 µW, ensuring scalability at 4.7 K. However, the measurements presented here were previously conducted at 1 mW without attenuation. Although results at 4.7 K are promising, further evaluation of photodiode performance at the milli-Kelvin stage is needed, where managing heat load becomes increasingly critical. This cryogenic system demonstrates a potential pathway for scaling quantum processors to support a significantly larger number of qubits.

Acknowledgment

This work is under the QSolid project and acknowledges the support of the Federal Ministry of Education and Research (BMBF) within the framework program “Quantum technologies – from basic research to market” (Grant No. 13N16149).

References

[1] S. Krinner, S. Storz, P. Kurpiers, P. Magnard, J. Heinsoo, R. Keller, J. Lütolf, C. Eichler, and A. Wallraff, “Engineering cryogenic setups for 100-qubit scale superconducting circuit systems,” *EPJ Quantum Technol.*, vol. 6, no. 1, p. 2, Dec. 2019. [Online]. Available: https://epjquantumtechnology.springeropen.com/articles/10.1140/epjqt/s40507-019-0072-0

[2] J. Yoo, Z. Chen, F. Arute, S. Montazeri, M. Szalay, C. Erickson, E. Jeffrey, R. Fatemi, M. Giustina, M. Ansmann, E. Lucero, J. Kelly, and J. C. Bardin, “Design and Characterization of a <4-mW/Qubit 28-nm Cryo-CMOS Integrated Circuit for Full Control of a Superconducting Quantum Processor Unit Cell,” *IEEE J. Solid-State Circuits*, vol. 58, no. 11, pp. 3044–3059, Nov. 2023. [Online]. Available: https://ieeexplore.ieee.org/document/10252147/

[3] P. Vliex, C. Degenhardt, C. Grewing, A. Kruth, D. Nielinger, S. Van Waasen, and S. Heinen, “Bias Voltage DAC Operating at Cryogenic Temperatures for Solid-State Qubit Applications,” *IEEE Solid-State Circuits Lett.*, vol. 3, pp. 218–221, 2020.

[4] F. Lecocq, F. Quinlan, K. Cicak, J. Aumentado, S. A. Diddams, and J. D. Teufel, “Control and readout of a superconducting qubit using a photonic link,” *Nature*, vol. 591, no. 7851, pp. 575–579, Mar. 2021. [Online]. Available: https://www.nature.com/articles/s41586-021-03268-x

[5] J. Capmany and D. Novak, “Microwave photonics combines two worlds,” *Nature Photon*, vol. 1, no. 6, pp. 319–330, Jun. 2007. [Online]. Available: https://www.nature.com/articles/nphoton.2007.89

[6] P. J. Winzer, D. T. Neilson, and A. R. Chraplyvy, “Fiber-optic transmission and networking: the previous 20 and the next 20 years [Invited],” *Opt. Express*, vol. 26, no. 18, p. 24190, Sep. 2018. [Online]. Available: https://opg.optica.org/abstract.cfm?URI=oe-26-18-24190

[7] K. Usami and Y. Nakamura, “A photonic link for quantum circuits,” *Nat Electron*, vol. 4, no. 5, pp. 323–324, May 2021.

[8] Y. Hishikawa, T. Takenouchi, M. Higa, K. Yamagoe, H. Ohshima, and M. Yoshita, “Translation of Solar Cell Performance for Irradiance and Temperature From a Single *I-V* Curve Without Advance Information of Translation Parameters,” *IEEE J. Photovoltaics*, vol. 9, no. 5, pp. 1195–1201, Sep. 2019. [Online]. Available: https://ieeexplore.ieee.org/document/8796411/

[9] S. Lischke, A. Peczek, J. S. Morgan, K. Sun, D. Steckler, Y. Yamamoto, F. Korndörfer, C. Mai, S. Marschmeyer, M. Fraschke, A. Krüger, A. Beling, and L. Zimmermann, “Ultra-fast germanium photodiode with 3-dB bandwidth of 265 GHz,” *Nat. Photon.*, vol. 15, no. 12, pp. 925–931, Dec. 2021. [Online]. Available: https://www.nature.com/articles/s41566-021-00893-w

[10] A. B. Sproul and M. A. Green, “Improved value for the silicon intrinsic carrier concentration from 275 to 375 K,” *Journal of Applied Physics*, vol. 70, no. 2, pp. 846–854, Jul. 1991. [Online]. Available: https://pubs.aip.org/jap/article/70/2/846/387688/Improved-value-for-the-silicon-intrinsic-carrier

[11] J. Mair, S. Kusuma, D. Liebau, L. Duipmans, L. Schreckenberg, P. Vliex, A. Zambanini, and S. V. Waasen, “Rapid Prototyping Platform for Integrated Circuits for Quantum Computing,” in *2024 20th International Conference on Synthesis, Modeling, Analysis and Simulation Methods and Applications to Circuit Design (SMACD)*. Volos, Greece: IEEE, Jul. 2024, pp. 1–4. [Online]. Available: https://ieeexplore.ieee.org/document/10745395/

[12] E. Bardalen, B. Karlsen, H. Malmbekk, M. N. Akram, and P. Ohlckers, “Evaluation of InGaAs/InP photodiode for high-speed operation at 4 K,” *Int. J. Metrol. Qual. Eng.*, vol. 9, p. 13, 2018. [Online]. Available: https://www.metrology-journal.org/10.1051/ijmqe/2018015

[13] X. Liu, J. Liu, F. He, R. Ma, X. Zhao, Q. Zhong, Y. Dong, and T. Hu, “Cryogenic Ge-on-Si avalanche photodiodes operating at 1550 nm wavelength,” in *Optical Fiber Communication Conference (OFC) 2024*. San Diego California: Optica Publishing Group, 2024, p. W2B.17. [Online]. Available: https://opg.optica.org/abstract.cfm?URI=OFC-2024-W2B.17